J. Hydrau., Coast. Environ. Eng., JSCE, No. 677/II-55, 189-203, 2001 May

APPLICATION OF THE EQUIVALENT FREQUENCY RESPONSE METHOD TO NONLINEAR RUNOFF SYSTEM

- ST. VENANT EQUATIONS AND RELATED MODELS -

Luai HAMOUDA[1] and Mutsuhiro FUJITA[2]

[1]Member of JSCE, Graduate Student, Dept. of Civil Eng., Hokkaido University
(North 13, West 8, Sapporo 060-8628, Japan)
[2]Fellow of JSCE, Dr. Eng., Professor, Dept. of Civil Eng., Hokkaido University
(North 13, West 8, Sapporo 060-8628, Japan)

This paper proposes a new approach using the Equivalent Frequency Response Method (EFRM) for analyzing St.Venant model for unsteady one-dimensional flow along with its related models such as kinematic wave, diffusion wave and gravity wave models with two different lower stream boundary conditions. It is possible to calculate the gain, time lag, and impulse response function by the proposed method. Moreover, a new criterion is presented for evaluating the validity of each model for a range of Froude and kinematic wave number based on the obtained impulse response function. Finally, this paper suggests the possibility of applications of EFRM to real runoff analysis.

Key Words: *equivalent frequency response, equivalent frequency transfer function, St.Venant equations, diffusion equation, kinematic equation.*

1.INTRODUCTION

Many models have been proposed for modeling overland flow on a plane subject to a lateral inflow or rainfall. Typical models are the St.Venant model and its related models such as kinematic, diffusion and gravity which are obtained from the St.Venant equations. The goodness of these models had been evaluated by two non-dimensional parameters F_0 and K, referred to as the Froude number and kinematic wave number respectively. Woolhiser and Liggett (1967)[1], Morris and Woolhiser (1980)[2], and Daluz Vieira (1983)[3] compared dimensionless hydrographs obtained from the above models using the square mean of differences between the St.Venant equations and its related models. In these works, the rising hydrographs obtained from different models were compared under assumption of constant rainfall. However the assumption of constant rainfall is very impractical.

In this paper, we proposed a method for calculating equivalent impulse response functions for the above mentioned models by introducing the equivalent frequency response method (EFRM), and we discuss the validity of each model on a $K-F_0$ plane. Originally, the EFRM was first used in control engineering for analyzing nonlinear elements such as threshold and saturation. The notion of EFRM had already been used by Fujita and Kudo (1995)[4], and Tanaka and Fujita (1998,1999)[5,6] to describe the characteristics of runoff models. These studies focused only on the gain characteristics of storage function model and kinematic wave model. We have developed a general EFEM which can deal with St.Venant model and its related models. Furthermore, we discuss a new possibility for analyzing runoff system using the EFRM.

2. ST. VENANT EQUATIONS AND RELATED MODELS

The full Saint Venant equations for describing the propagation of shallow waves over a plane surface are given by

$$\frac{\partial h}{\partial t}+\frac{\partial q}{\partial x}=r \qquad 0\le x\le l \tag{1}$$

$$\frac{\partial u}{\partial t}+u\frac{\partial u}{\partial x}+g\frac{\partial h}{\partial x}=g\left(s_0-s_f\right)-\frac{ru}{h} \tag{2}$$

x, t : space and time coordinates
h, u, q : depth, velocity, and discharge at (x,t)
l : length of the plane
r : rainfall intensity
g : acceleration due to gravity
s_0 : slope of the plane
s_f : friction slope defined by Chezy equation

$$s_f = \frac{u^2}{C^2 h} \tag{3}$$

C : Chezy roughness of the plane

These equations can be written in non-dimensional form by introducing the following normalizing quantities, denoted by the subscript $(*)$.

$$x_* = \frac{x}{X}, h_* = \frac{h}{H}, u_* = \frac{u}{U}, t_* = \frac{t}{T}, r_* = \frac{r}{R}, q_* = \frac{q}{Q} \tag{4}$$

The capital letters (such as H) denote non-dimensional quantities corresponding to dimensional quantities (such as h).
The following two conditions were adopted.

$$x_* = l \tag{5}$$

$$r_* = \bar{r} \tag{6}$$

$\bar{r}$: average rainfall intensity

By substituting eqs.(4), (5) and (6) into eqs.(1) and (2), the following equations can be obtained.

$$h_* = \frac{\bar{r} l}{u_*} = \left\{\frac{\bar{r} l}{C\sqrt{s_0}}\right\}^{2/3} \tag{7}$$

$$u_* = \frac{\bar{r} l}{h_*} = C\sqrt{s_0}\left\{\frac{\bar{r} l}{C\sqrt{s_0}}\right\}^{1/3} \tag{8}$$

$$t_* = \frac{h_*}{\bar{r}} = \frac{1}{r}\left\{\frac{\bar{r} l}{C\sqrt{s_0}}\right\}^{2/3} \tag{9}$$

$$\frac{g h_* t_*}{u_* l} = \frac{g h_*}{u_*^2} = \frac{g}{C^2 s_0} = \frac{1}{F_0^2} \tag{10}$$

$$\frac{g s_0 t_*}{u_*} = \frac{g\sqrt{s_0}}{C\bar{r}}\left\{\frac{\bar{r} l}{C\sqrt{s_0}}\right\}^{1/3} = K \tag{11}$$

Original paper, Woolhiser and Liggett (1967), used r_{max} (maximum rainfall) instead of $\bar{r}$. However this new normalizing parameter $\bar{r}$ would not affect their results because r_{max} should be equal to $\bar{r}$ under the assumption of constant rainfall. Finally, eqs.(1) and (2) can be rewritten in a non-dimensional form.

$$\frac{\partial H}{\partial T} + \frac{\partial Q}{\partial X} = R \qquad 0 \le X \le L \tag{12}$$

$$\frac{\partial U}{\partial T} + U\frac{\partial U}{\partial X} + \frac{1}{F_0^2}\frac{\partial H}{\partial X} = K\left(1 - \frac{U^2}{H}\right) - \frac{RU}{H} \tag{13}$$

L : non-dimensional slope length. $L = 1$

The two independent parameters are the Froude number (F_0) and the kinematic wave number (K).

Several types of momentum equations can be derived from eq. (13). The momentum equation of the kinematic wave model is

$$U = \sqrt{H} \qquad \text{or} \qquad Q = H^{3/2} \tag{14}$$

Also, the momentum equation of the diffusion model is

$$U = H^{1/2}\left(1 - \frac{1}{F_0^2 K}\frac{\partial H}{\partial X}\right)^{1/2} \tag{15}$$

Finally, the momentum equation of the gravity model is

$$\frac{\partial U}{\partial T} + U\frac{\partial U}{\partial X} + \frac{1}{F_0^2}\frac{\partial H}{\partial X} = -\frac{RU}{H} \tag{16}$$

Furthermore, several storage function runoff models based on the kinematic wave model have been proposed by Fujita (1981)[7] and Hoshi (1982)[8].

$$\frac{dS}{dT} + Q_H = R \tag{17}$$

$$S = K_1 Q_H^{p_1} \tag{18}$$

$$S = K_1 Q_H^{p_1} + K_2 \frac{dQ_H^{p_2}}{dT} \tag{19}$$

S : nondimensional storage
Q_H : nondimensional depth of runoff
K_1, K_2, p_1, p_2 : constants

3. EQUIVALENT FREQUENCY RESPONSE ANALYSIS

In this section, an extended form of the ordinary frequency response function, called the equivalent frequency response method (EFRM) is introduced to evaluate the output from nonlinear runoff models.

(1) Equivalent frequency response for storage function model

As eq.(18) is a special case of eq.(19), we adopt eq.(19).

$$\frac{dS}{dT} + Q_H = R \tag{20}$$

$$S = K_1 Q_H^{p_1} + K_2 \frac{dQ_H^{p_2}}{dT} \tag{21}$$

Hoshi (1982) defined the following coefficients obtained from the nondimensional kinematic wave eqs.(12) and (14).

$$p = \frac{3}{2} \quad p_1 = \frac{1}{p} \quad p_2 = p_1^{1.5}$$
$$K_1 = \frac{1}{p_1 + 1} \quad K_2 = 0.1 p_1^{-0.2} \tag{22}$$

In order to obtain the equivalent frequency transfer function between $R(T)$ and $Q_H(T)$, we assume that

$$R(T) = \overline{R} + Ae^{j\Omega T} \tag{23}$$

$$Q_H(T) = \overline{Q}_H + Ce^{j\Omega T} \tag{24}$$

$\overline{R}, \overline{Q}_H$: nondimensional average rainfall and depth of runoff A, C : constants

j : imaginary unit Ω : nondimensional frequency

The relationship between Ω and ordinary frequency ω is expressed by

$$\Omega = \omega t_* \tag{25}$$

Nonlinear terms in eq.(21) are approximated by

$$Q_H^{P_1} \approx \overline{Q}_H^{P_1}\left(1 + \frac{p_1 C}{\overline{Q}_H} e^{j\Omega T}\right) \tag{26}$$

$$Q_H^{P_2} \approx \overline{Q}_H^{P_2}\left(1 + \frac{p_2 C}{\overline{Q}_H} e^{j\Omega T}\right) \tag{27}$$

Substituting eqs.(26) and (27) into eqs.(20) and (21) yields

$$\overline{Q}_H = \overline{R} \tag{28}$$

$$Z_s(j\Omega) = \frac{C}{A} = \frac{1}{1 - \Omega^2 K_2 p_2 \overline{R}^{P_2 - 1} + j\Omega K_1 p_1 \overline{R}^{P_1 - 1}}$$
$$= R_e[Z_s(j\Omega)] + jI_m[Z_s(j\Omega)] \tag{29}$$

$$R_e[Z_s(j\Omega)] = \frac{1}{\left(1 - \Omega^2 K_2 p_2 \overline{R}^{P_2 - 1}\right)^2 + \left(\Omega K_1 p_1 \overline{R}^{P_1 - 1}\right)^2} \tag{30}$$

$$I_m[Z_s(j\Omega)] = \frac{-\Omega K_1 p_1 \overline{R}^{P_1 - 1}}{\left(1 - \Omega^2 K_2 p_2 \overline{R}^{P_2 - 1}\right)^2 + \left(\Omega K_1 p_1 \overline{R}^{P_1 - 1}\right)^2} \tag{31}$$

$Z_s(j\Omega)$ indicates the equivalent frequency transfer function between $R(T)$ and $Q_H(T)$. $R_e[Z_s(j\Omega)]$ and $I_m[Z_s(j\Omega)]$ denote real and imaginary components of $Z_s(j\Omega)$, respectively. The gain and time lag functions are defined by

$$G_s(\Omega) = |Z_s(j\Omega)| \tag{32}$$

$$T_{Ls}(\Omega) = \frac{Arg[Z_s(j\Omega)]}{\Omega} \tag{33}$$

The relationship between $R(T)$ and $Q_H(T)$ can be derived from eq.(29).

$$K_2 p_2 \overline{R}^{P_2 - 1} \frac{d^2 Q_H}{dT^2} + K_1 p_1 \overline{R}^{P_1 - 1} \frac{dQ_H}{dT} + Q_H = R \tag{34}$$

On the other hand, eq.(35) is derived from eqs.(20) and (21).

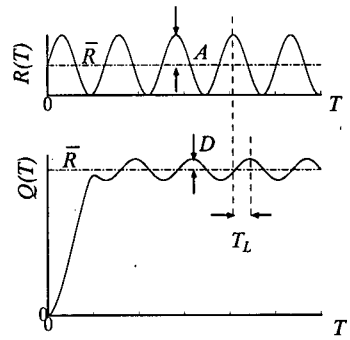

Fig.1 Schematic relationship between sinusoidal input and its output

$$K_2 p_2 \overline{Q}_H^{P_2 - 1} \frac{d^2 Q_H}{dT^2} + K_2 p_2 (p_2 - 1) \overline{Q}_H^{P_2 - 2} \left(\frac{dQ_H}{dT}\right)^2$$
$$+ K_1 p_1 \overline{Q}_H^{P_1 - 1} \frac{dQ_H}{dT} + Q_H = R \tag{35}$$

The above nonlinear differential equation (35), is converted into a semi linear differential equation (34). The word "semi" means that eq.(34) is not a completely linear equation since its coefficients are affected by rainfall input. As eq.(34) is derived by the EFRM, its rainfall inputs are limited to sinusoidal functions. However, any arbitrary time function can be described by sinusoidal functions through a Fourier series as

$$R(T) = \overline{R} + \sum_{n=1}^{\infty} \{\alpha_n \cos(n\Omega_0 T) - \beta_n \sin(n\Omega_0 T)\} \tag{36}$$

$$\Omega_0 = \frac{2\pi}{T_p} \qquad \overline{R} = \frac{1}{T_p} \int_0^{T_p} R(T) dT \tag{37}$$

$$\alpha_n = \frac{1}{T_p} \int_0^{T_p} R(T) \cos(n\Omega_0 T) dT \tag{38}$$

$$\beta_n = \frac{1}{T_p} \int_0^{T_p} R(T) \sin(n\Omega_0 T) dT \tag{39}$$

Therefore, the limitation to a sinusoidal input does not matter in practical application. The original definition of T_p is the period of $R(T)$. In this paper, we define T_p as the duration of runoff. $Q_H(T)$ can be derived from eqs.(32), (33) and (36).

$$Q_H(T) = \overline{R} + 2 \sum_{n=1}^{\infty} G(n\Omega_0) [\alpha_n \cos\{n\Omega_0 (T - T_{Ls}(n\Omega_0))\}$$
$$- \beta_n \sin\{n\Omega_0 (T - T_{Ls}(n\Omega_0))\}] \tag{40}$$

Equations (26) and (27) are approximations. The accuracy of eq.(29) is cross-checked by a numerical method, assuming the following rainfall.

$$R(T) = \overline{R} + A\sin(\Omega T) \tag{41}$$

A : constant amplitude

Figure 1 shows the schematic relationship between a sinusoidal input and its output. The gain function is calculated numerically as

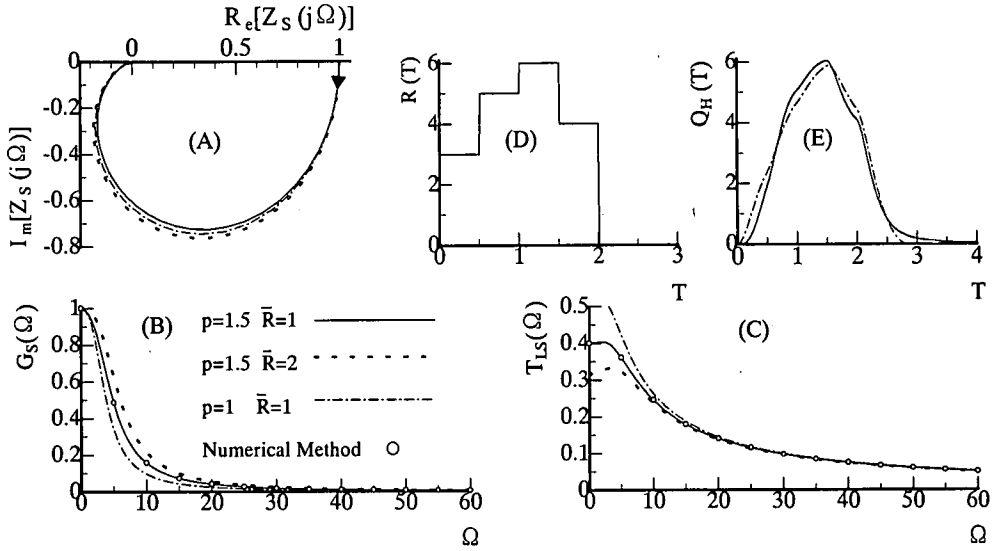

Fig.2 Storage function model

$$G(\Omega) = \frac{D}{A} \tag{42}$$

The time lag function $T_L(\Omega)$ is calculated by the time interval between both sinusoidal peaks as shown in **Fig.1**. **Figure 2** (A), (B) and (C) show the vector locus [eq.(29)] (relationship between $R_e[Z(j\Omega)]$ and $I_m[Z(j\Omega)]$), gain function [eq.(32)], and time lag function [eq.(33)] for $p=1.5$ and $\bar{R}=1$ (solid line), $p=1.5$ and $\bar{R}=2$ (dotted line), and $p=1$ and $\bar{R}=1$ (dashed line). The circles in (B) and (C) show the numerical results obtained from eqs.(35) and (41). Numerical results agree with theoretical ones. Also, **Fig.2** (E) shows a comparison between the solutions obtained from eqs.(35) (solid line) and (34) (dashed line) using rainfall input (D).
The two solutions are almost the same. Furthermore, we add eq.(40) completely coincides with the solution of eq.(34).

(2) Equivalent frequency response for kinematic wave model

Kinematic wave model is expressed by

$$\frac{\partial H}{\partial T} + \frac{\partial Q}{\partial X} = R \qquad 0 \le X \le L \tag{43}$$

$$Q = H^p \tag{44}$$

This model has only one parameter p . $p=1.5$ corresponds to St. Venant model. Boudary and initial conditions are

$$H(T,0) = 0,\ Q(T,0) = 0 \tag{45}$$

$$H(0,X) = 0,\ Q(0,X) = 0 \tag{46}$$

In order to obtain the equivalent frequency transfer function between $R(T)$ and $Q(T,1)$, we define eqs.(23), (47) and (48).

$$H(T,X) = \bar{H}(X) + B(X)e^{j\Omega T} \tag{47}$$

$$Q(T,X) = \bar{Q}(X) + C(X)e^{j\Omega T} \tag{48}$$

$\bar{H}(X)$ *and* $\bar{Q}(X)$: water depth and discharge in the steady state respectively
$B(X)$ *and* $C(X)$: complex functions
We obtain eqs.(49) and (50) from eqs.(23), (43), (47) and (48).

$$\bar{Q}(X) = \bar{R}X \tag{49}$$

$$\frac{dC}{dX} + j\Omega B = A \tag{50}$$

Equations (51) and (52) are derive from eqs.(44), (47) and (48) using a similar approximation as that of eq.(26).

$$\bar{Q}(X) = \bar{H}^p \tag{51}$$

$$C(X) = p\bar{H}^{p-1}B(X) \tag{52}$$

We finally obtain eq.(53).

$$\frac{dC}{dX} + jp_1\Omega(\bar{R}X)^{p_1-1}C = A \qquad p_1 = \frac{1}{p} \tag{53}$$

The boundary condition in eq.(45) suggests

$$C(0) = 0 \tag{54}$$

The solution of eq.(53) is

$$C(X) = Ae^{-j\Omega\bar{R}^{p_1-1}X^{p_1}} \int_0^X e^{j\Omega\bar{R}^{p_1-1}X_1^{p_1}} dX_1 \tag{55}$$

The equivalent frequency transfer function between $R(T)$ and $Q(T,1)$ is expressed by

$$Z_k(j\Omega) = \frac{C(1)}{AL} \tag{56}$$

We rewrite eq.(56).

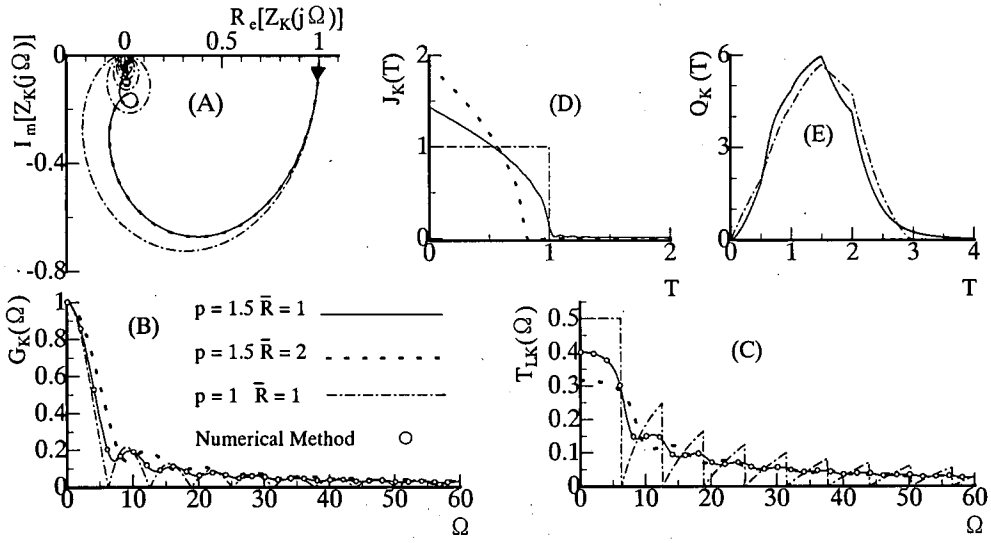

Fig.3 Kinematic wave model

$$Z_k(j\Omega) = R_e[Z_k(j\Omega)] + jI_m[Z_k(j\Omega)] \tag{57}$$

$$R_e[Z_k(j\Omega)] = \frac{1}{L}\{I_1\cos(\Omega\lambda_1) + I_2\sin(\Omega\lambda_1)\} \tag{58}$$

$$I_m[Z_k(j\Omega)] = \frac{1}{L}\{I_2\cos(\Omega\lambda_1) - I_1\sin(\Omega\lambda_1)\} \tag{59}$$

$$I_1 = \int_0^L \cos(\Omega\lambda_2 X^{p_1})dX$$

$$= \frac{1}{2}\{{}_1F_1(p, p+1, j\Omega\lambda_1) + {}_1F_1(p, p+1, -j\Omega\lambda_1)\} \tag{60}$$

$$I_2 = \int_0^L \sin(\Omega\lambda_2 X^{p_1})dX$$

$$= -\frac{j}{2}\{{}_1F_1(p, p+1, j\Omega\lambda_1) - {}_1F_1(p, p+1, -j\Omega\lambda_1)\} \tag{61}$$

$$\lambda_1 = \bar{R}^{p_1-1}L^{p_1} \qquad \lambda_2 = \bar{R}^{p_1-1} \tag{62}$$

${}_1F_1(\eta,\kappa,\gamma)$ shows Kummer's confluent hypergeometric function defined as

$${}_1F_1(\eta,\kappa,\gamma) = 1 + \frac{\eta\gamma}{\kappa} + \frac{\eta(\eta+1)\gamma^2}{2!\kappa(\kappa+1)} + \frac{\eta(\eta+1)(\eta+2)\gamma^3}{3!\kappa(\kappa+1)(\kappa+2)} + \tag{63}$$

If $p = 1$, then eq.(56) is

$$Z_k(j\Omega) = \frac{1}{L}\left\{\frac{\sin(\Omega)}{\Omega} + j\frac{\cos(\Omega)-1}{\Omega}\right\} \tag{64}$$

$Z_k(j\Omega)$ in eq.(64) is independent of its average rainfall input. The gain and time lag functions are defined by

$$G_k(\Omega) = |Z_k(j\Omega)| \tag{65}$$

$$T_{Lk}(j\Omega) = \frac{Arg[Z_k(j\Omega)]}{\Omega} \tag{66}$$

It is impossible to derive a differential equation corresponding to $Z_k(j\Omega)$ in eq.(56) because $Z_k(j\Omega)$ is obtained numerically. We define the equivalent impulse response function $J_k(T)$ instead of a differential equation.

$$J_k(T) = \frac{2}{\pi}\int_0^\infty R_e[Z_k(j\Omega)]\cos(\Omega T)d\Omega \tag{67}$$

Figure 3 (A),(B),(C) and (D) show vector locus [eq.(56)], the gain function [eq.(65)], time lag function [eq.(66)], and impulse response function [eq.(67)] for $p = 1.5$ and $\bar{R} = 1$ (solid line), $p = 1.5$ and $\bar{R} = 2$ (dotted line), and $p = 1$ and $\bar{R} = 1$ (dashed line). The circles in (B) and (C) show the numerical results obtained by eqs.(41), (43) and (44), as explained before. It was found that eqs.(65) and (66) are very accurate. The gain and time lag functions show wavy fluctuations. These phenomena are explained by the linear kinematic wave equation. The impulse response function corresponding to $p = 1$ is rectangular in shape as shown in **Fig.3** (D). $Q(T,1)$ is calculated by

$$Q(T,1) = \int_{T-1}^{T} R(\tau)d\tau \tag{68}$$

We obtain eq.(69) by substituting eq.(23) into eq.(68).

$$Q(T,1) = \bar{R} + A\sqrt{2(1-\cos(\Omega))}\sin(\Omega T + \phi) \tag{69}$$

$$\tan(\phi) = \frac{\cos(\phi)-1}{\sin(\phi)} \tag{70}$$

The amplitude and phase of eq.(69) becomes 0 at $\Omega = 2n\pi, n = 1,2,$. This tendency is maintained in the case of $p = 1.5$ because the impulse response function for $p = 1.5$ resembles the rectangular shape for $p = 1$.
Also **Fig.3** (E) shows a comparison of solutions obtained from eqs.(43) and (44) (solid line) and eq.(67) (dashed line) using the previously mentioned rainfall in **Fig.2** (D). The solution shows good agreement.

(3) Equivalent frequency response for diffusion wave model

Table 1 shows the summary of the EFRM for diffusion wave model with two kinds of lower boundary conditions. This model is defined by eqs.(71) and (72) in **Table 1**. The upper boundary and initial conditions are

$$Q(T,0) = 0 \tag{73}$$

$$Q(0,X) = 0 \tag{74}$$

The lower boundary conditions are discussed later.
We used the same equations [eqs.(23), (47) and (48)] to derive the frequency transfer function between $R(T)$ and $Q(T,1)$. $\overline{Q}(X)$ and $\overline{H}(X)$ in the steady state are expressed by eqs.(75) and (76) in **Table 1**.

The nonlinear terms in eq.(72) are approximated by

$$Q \approx H^{3/2}\left(1-\frac{1}{2F_0^2K}\frac{\partial H}{\partial X}\right) \tag{77}$$

$$H^{3/2} \approx \overline{H}^{3/2}\left(1+\frac{3B}{2\overline{H}}e^{j\Omega T}\right) \tag{78}$$

We can derive eqs.(79) and (80) from eqs.(23), (47), (48), (77) and (78) together with eqs.(71) and (72) by extracting the fundamental components.

$$\frac{dC}{dX} + j\Omega B = A \tag{79}$$

$$\frac{dB}{dX} = \frac{1}{2\overline{H}^{3/2}}\left\{F_0^2K\left(6B\overline{H}^{1/2}-4C\right)-3B\overline{H}^{1/2}\frac{d\overline{H}}{dX}\right\} \tag{80}$$

Equations (81), (82), (83) and (84) are obtained after eliminating B from eqs.(79) and (80).

$$f_1 = \frac{1}{2\overline{H}}\left(3\frac{d\overline{H}}{dX}-6F_0^2K\right) \tag{82}$$

$$f_2 = -\frac{2jF_0^2K\Omega}{\overline{H}^{3/2}} \tag{83}$$

$$f_3 = Af_1 \tag{84}$$

Equation (73) leads to eq.(85) in **Table 1**.

a) Zero-depth-gradient lower boundary condition

This condition defined as

Table 1 Diffusion model's summary

Unsteady State	Steady State
$\frac{\partial H}{\partial T}+\frac{\partial Q}{\partial X}=R$ (71) $(0 \le X \le L)$ $Q = H^{3/2}\left(1-\frac{1}{F_0^2K}\frac{\partial H}{\partial X}\right)^{1/2}$ (72)	$\overline{Q}(X) = \overline{R}X$ (75) $\frac{d\overline{H}}{dX} = \frac{F_0^2K(\overline{H}^3-\overline{R}^2X^2)}{\overline{H}^3}$ (76) $\overline{H}_1 = \overline{H}_Z(1)$ *or* $\overline{H}_C(1)$
$\frac{d^2C}{dX^2}+f_1\frac{dC}{dX}+f_2C=f_3$ (81)	
Zero Depth Condition $C(0)=0$ (85) $\left[\frac{d^2C}{dX^2}\right]_{X=1}=0$ (90)	$\overline{H}_Z(1) = (\overline{R}L)^{2/3}$ (89)
Critical Flow Condition $C(0)=0$ (85) $\left[\frac{d^2C}{dX^2}\right]_{X=1}=0$ (90)	$\overline{H}_C(1) = (\overline{R}LF_0)^{2/3}$ (92)

$$\left[\frac{\partial H}{\partial X}\right]_{X=1} = 0 \tag{86}$$

Equations (87) and (88) are derived from eq.(86) .

$$\left[\frac{d\overline{H}}{dX}\right]_{X=1} = 0 \tag{87}$$

$$\left[\frac{dB}{dX}\right]_{X=1} = 0 \tag{88}$$

Equations (76) and (87) lead to eq.(89) in **Table 1**. We can derive eq.(90) in **Table 1** from eqs.(79) and (88).

b) Critical flow lower boundary condition

This condition is defined as

$$Q(T,1) = \frac{H^{3/2}(T,1)}{F_0} \tag{91}$$

It is reasonable to assume that $\overline{Q}(T,1)$ and $\overline{H}(T,1)$ satisfy eq.(91), and eq.(91) leads to eq.(92) in **Table1**. Equation (93) is derived from eqs.(72) and (91).

$$\left[\frac{\partial H}{\partial X}\right]_{X=1} = K\left(F_0^2-1\right) \tag{93}$$

We obtain eq.(94) from eqs.(76) and (92).

$$\left[\frac{d\overline{H}}{dX}\right]_{X=1} = K\left(F_0^2-1\right) \tag{94}$$

From eqs.(94) and (93) we can conclude that

$$\left[\frac{dB}{dX}\right]_{X=1} = 0 \tag{95}$$

Equations (95) and (88) are the same. Therefore, we adopt eq.(90) as the boundary condition for $C(X)$ at

Table 2 St.Venant model's summary

Unsteady State	Steady State
$\frac{\partial H}{\partial T}+\frac{\partial Q}{\partial X}=R \qquad 0\le X\le 1$ (99) $\frac{\partial U}{\partial T}+U\frac{\partial U}{\partial X}+\frac{1}{F_0^2}\frac{\partial H}{\partial X}=K\left(1-\frac{U^2}{H}\right)-\frac{RU}{H}$ (100)	$\overline{Q}=\overline{U}\,\overline{H}=\overline{R}X$ (102) $\frac{d\overline{H}}{dX}=\frac{K\left(\overline{H}^3-\overline{R}^2X^2\right)-2\overline{R}^2\overline{H}X}{\frac{\overline{H}^3}{F_0^2}-\overline{R}^2X^2}$ (103)
$\frac{d^2C}{dX^2}+f_1\frac{dC}{dX}+f_2C=f_3$ (106)	
Zero Depth Condition $C(0)=0$ (110) $\left[\frac{d^2C}{dX^2}\right]_{X=1}=0$ (111)	$\frac{d\overline{H}}{dX}=\frac{K\left(\overline{H}^3-\overline{R}^2X^2\right)-2\overline{R}^2\overline{H}X}{\frac{\overline{H}^3}{F_0^2}-\overline{R}^2X^2}$ $\overline{H}_Z(1)\ge\overline{H}_C(1)$ $\overline{H}(1)=\overline{H}_Z(1)$ (117) *No Solution* $\overline{H}_Z(1)<\overline{H}_C(1)$
Critical Flow Condition $C(0)=0$ (110) $\left[\frac{dC}{dX}\right]_{X=1}=\frac{A(-3+V_1)}{(1+V_1)}$; $V_1=\left[\frac{KF_0}{\sqrt{\overline{H}}}\left(1-\frac{1}{F_0^2}\right)\frac{1}{j\Omega}\right]_{X=1}$ (116)	$\frac{d\overline{H}}{dX}=\frac{K\left(\overline{H}^3-\overline{R}^2X^2\right)-2\overline{R}^2\overline{H}X}{\frac{\overline{H}^3}{F_0^2}-\overline{R}^2X^2}$ $\overline{H}_Z(1)\ge\overline{H}_C(1)$ $\overline{H}(1)=\overline{H}_C(1)$ (117) *No Solution* $\overline{H}_Z(1)<\overline{H}_C(1)$

$X=1$. The boundary conditions of eq.(81) are the same concerning the zero-depth-gradient and critical flow lower boundary condition and eq.(81) is a boundary value problem. The difference between the two lower boundary conditions appears in $\overline{H}(1)$ expressed by eqs.(89) and (92). $\overline{H}(X)$ can be derived by solving eq.(76) along with eqs.(89) or (92) then eqs.(82), (83) and (84) are calculated to derive f_1, f_2 and f_3 respectively. The equivalent frequency transfer function between $R(T)$ and $Q(T,1)$ is defined as

$$Z_D(j\Omega)=\frac{C(1)}{AL} \tag{96}$$

The gain and time lag functions are

$$G_D^Z(\Omega) \text{ or } G_D^C(\Omega)=|Z_D(j\Omega)| \tag{97}$$

$$T_{LD}^Z(\Omega) \text{ or } T_{LD}^C(\Omega)=\frac{Arg[Z_D(j\Omega)]}{\Omega} \tag{98}$$

The upper suffixes such as Z and C denote the zero-depth-gradient and critical flow boundary condition. **Figure 4** (A),(B),(C) and (D) show the vector locus, gain, time lag and impulse response functions for the zero-depth-gradient and critical flow lower boundary conditions with $F_0^2K=5$ and $\overline{R}=1$ (solid line), $F_0^2K=5$ and $\overline{R}=2$ (dotted line), and $F_0^2K=50$ and $\overline{R}=1$ (dashed line). The circles in (B) and (C) show numerical results, as explained before. The numerical results agree with the theoretical ones. Also, **Fig.4** (E) shows a comparison of the solutions obtained from eqs.(71) and (72) (solid line) and the solution obtained from the impulse response function (dashed line) using the previously mentioned rainfall in **Fig.2** (D) for both lower boundary conditions. The solutions show good agreement.

(4) Equivalent frequency response for the St. Venant model

Table 2 shows a summary of the EFRM for the St.Venant model with two kinds of lower boundary conditions. This model is defined by eqs.(99) and (100) in **Table 2.** The upper boundary and initial conditions are expressed by the same equations [eqs.(73) and (74)]. The lower boundary conditions are discussed later.

Rewriting eq.(100) yields

$$H^2\frac{\partial Q}{\partial T}-2QH\frac{\partial H}{\partial T}+\left(\frac{H^3}{F_0^2}-Q^2\right)\frac{\partial H}{\partial X}=K\left(H^3-Q^2\right)-2RQH \tag{101}$$

We use the same equations [eqs.(23), (47) and (48)] in order to derive the frequency transfer function between $R(T)$ and $Q(T,1)$. $\overline{Q}(X)$ and $\overline{H}(X)$ in the steady state are expressed by eqs.(102) and (103) in **Table 2.** We can derive eqs.(104) and (105) from eqs.(23), (47) and (48) along with eqs. (99) and (101) by extracting the fundamental components.

$$\frac{dC}{dX}+j\Omega B=A \tag{104}$$

$$\frac{dB}{dX}=\left\{\overline{H}F_0^2\left(3KB\overline{H}-2\overline{R}C-j\Omega C\overline{H}\right)+2F_0^2\overline{Q}\left(j\Omega B\overline{H}-\overline{R}B-KC-A\overline{H}\right)+\left(2F_0^2C\overline{Q}-3B\overline{H}^2\right)d\overline{H}/dX\right\}\Big/\left(\overline{H}^3-F_0^2\overline{Q}^2\right) \tag{105}$$

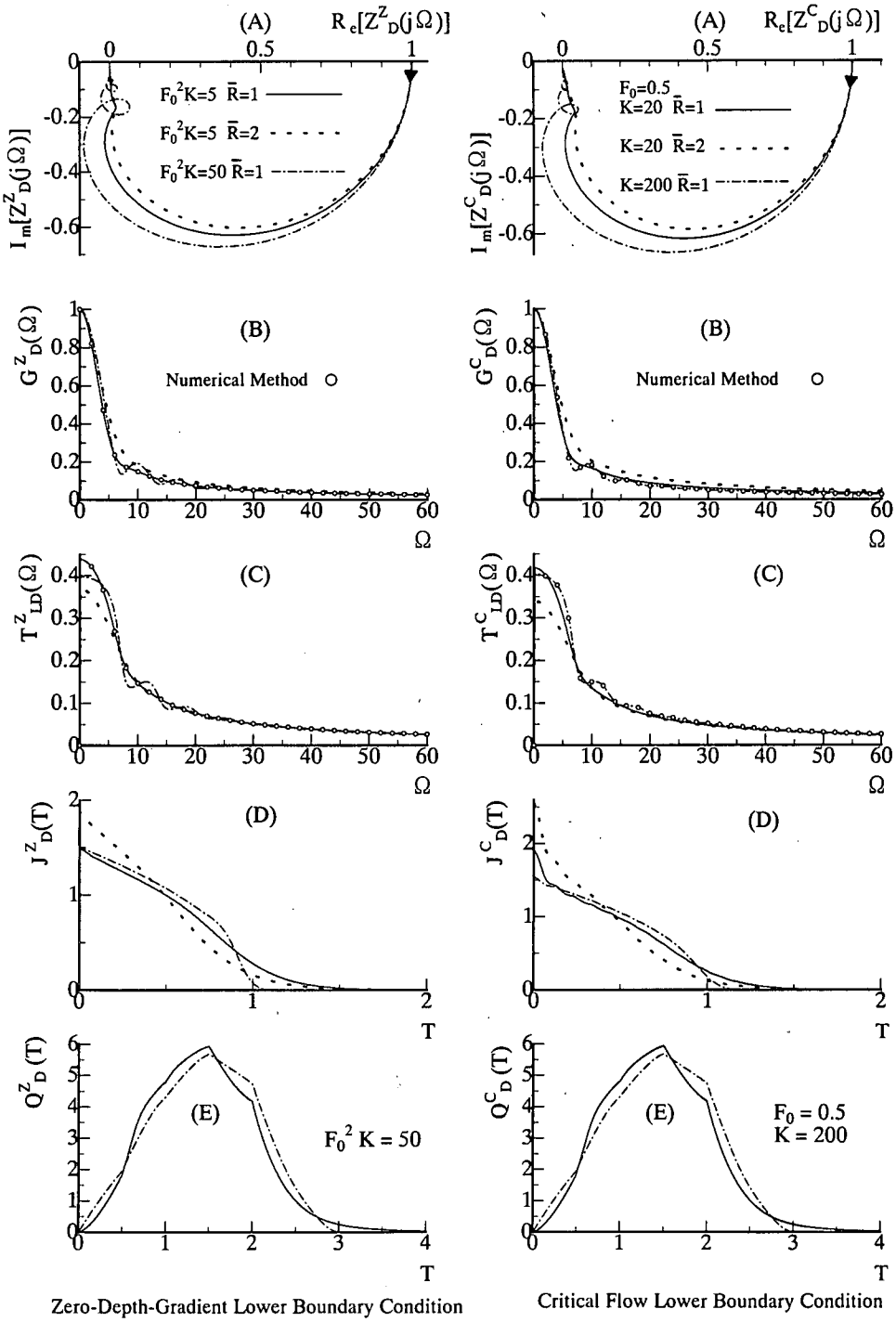

Fig.4 Diffusion wave model

Equations (106), (107), (108) and (109) are obtained after eliminating B from eqs.(104) and (105).

$$f_1=\frac{F_0^2\left(3K\overline{H}^2+2j\Omega\overline{H}\,\overline{Q}-2\overline{R}\,\overline{Q}\right)-3\overline{H}^2\left(d\overline{H}/dX\right)}{F_0^2\overline{Q}^2-\overline{H}^3} \qquad (107)$$

$$f_2=\frac{2jF_0^2\Omega\left\{\overline{R}\,\overline{H}+K\overline{Q}-\overline{Q}\left(d\overline{H}/dX\right)\right\}-F_0^2\Omega^2\overline{H}^2}{F_0^2\overline{Q}^2-\overline{H}^3} \qquad (108)$$

$$f_3=\frac{F_0^2A\left(3K\overline{H}^2-2\overline{R}\,\overline{Q}\right)-3A\overline{H}^2\left(d\overline{H}/dX\right)}{F_0^2\overline{Q}^2-\overline{H}^3} \qquad (109)$$

Equation (74) gives eq.(110) in **Table 2.**

a) Zero-depth-gradient condition

This condition is expressed by eq.(86). Eqs.(87) and (88) are used here. Eq.(111) in **Table 2** is derived from eqs.(104) and eq.(88). Eqs.(87) and (103) lead to eq.(112).

b) Critical flow condition

This condition is defined by eq.(91).

$$\begin{cases}\overline{H}_Z(1)=\dfrac{2^{4/3}\overline{R}^2}{V^{1/3}}+\dfrac{V^{1/3}}{3\left(2^{1/3}\right)K} & for \quad 32\overline{R}^2\le 27K^3\\ V=27K^3\overline{R}^2+\sqrt{729K^6\overline{R}^4-864K^3\overline{R}^6} & for \quad 32\overline{R}^2>27K^3\\ \overline{H}_Z(1)=2\overline{R}\sqrt{\dfrac{2}{3K}}Cos\left\{\dfrac{1}{3}\tan^{-1}\left(\sqrt{\dfrac{32\overline{R}^2}{27K^3}-1}\right)\right\}\end{cases} \qquad (112)$$

Equation (113) is derived from eqs.(102) and (91).

$$\overline{H}(1)=\left(F_0\,\overline{R}\right)^{2/3} \qquad (113)$$

Equation (91) leads to eq.(114).

$$\left[\frac{\partial Q}{\partial T}\right]_{X=1}=\left[\frac{3}{2}\frac{\sqrt{H}}{F_0}\frac{\partial H}{\partial T}\right]_{X=1} \qquad (114)$$

Equation (99) and (101) along with eqs.(91) and (114) lead to

$$\left[\frac{\partial Q}{\partial X}\right]_{X=1}=\left[-3R+2KF_0\left(1-\frac{1}{F_0^2}\right)\sqrt{H}\right]_{X=1} \qquad (115)$$

After substituting eqs.(23), (47), (48) and (104) into eq.(115) and extracting the fundamental component, we obtain eq.(116) in **Table 2.**

$\overline{H}(X)$ is expressed by eq.(117) in **Table 2.**

As it is impossible to solve eq.(103) under the condition of $\overline{H}_Z(1)<\overline{H}_C(1)$, we employ eq.(117) in **Table 2** to calculate $\overline{H}(X)$. **Figure 5** shows the zone for the condition $\overline{H}_Z(1)>\overline{H}_C(1)$ for $\overline{R}=1$ (solid line), $\overline{R}=2$ (dashed line), and $\overline{R}=1/2$ (dotted line) in the K - F_0 field.

In the same way as that used in the diffusion wave model, the equivalent frequency transfer function between $R(T)$ and $Q(T,1)$ is defined as

$$Z_{SV}(j\Omega)=\frac{C(1)}{AL} \qquad (118)$$

The gain and time lag functions are

$$G_{SV}^{Z}(\Omega)\ or\ G_{SV}^{C}(\Omega)=\left|Z_{SV}(j\Omega)\right| \qquad (119)$$

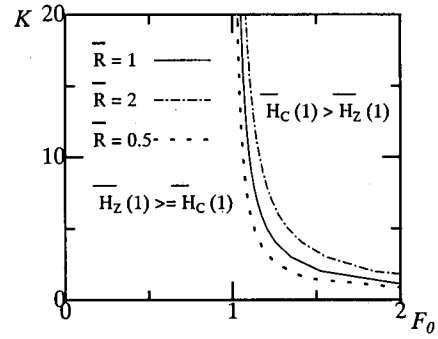

Fig.5 Validity zone of St. Venant model in K - F_0 field

$$T_{LSV}^{Z}(\Omega)\ or\ T_{LSV}^{C}(\Omega)=\frac{Arg[Z_{SV}(j\Omega)]}{\Omega} \qquad (120)$$

Figure 6 (A),(B),(C) and (D) shows the vector locus, gain, time lag and impulse response functions for the zero-depth-gradient and critical flow lower boundary conditions with $F_0^2K=5$ and $\overline{R}=1$ (solid line) , $F_0^2K=5$ and $\overline{R}=2$ (dotted line), and $F_0^2K=50$ and $\overline{R}=1$ (dashed line). The circles in (B) and (C) indicate numerical results as explained before. Numerical results agree with theoretical ones. Also **Fig.6** (E) shows a comparison between solutions obtained from eqs.(99) and (100) (solid line) and solution from impulse response function (dashed line) using the previous mentioned rainfall for both lower boundary conditions. Solutions show good agreements.

(5) Equivalent frequency response for gravity wave model

The gravity wave model is defined by the following continuity and momentum equations.

$$\frac{\partial H}{\partial T}+\frac{\partial Q}{\partial X}=R \qquad 0\le X\le L \qquad (121)$$

$$\frac{\partial U}{\partial T}+U\frac{\partial U}{\partial X}+\frac{1}{F_0^2}\frac{\partial H}{\partial X}=-\frac{RU}{H} \qquad (122)$$

The upper boundary and initial conditions are expressed by the same equations [eqs.(73) and(74)]. The lower boundary conditions are discussed later. The gravity wave model is a special case of the St.Venant model for $K=0$.

Eq.(101) leads to eq.(123).

$$H^2\frac{\partial Q}{\partial T}-2QH\frac{\partial H}{\partial T}+\left(\frac{H^3}{F_0^2}-Q^2\right)\frac{\partial H}{\partial X}=-2RQH \qquad (123)$$

In the steady state, $\overline{Q}(X)$ and $\overline{H}(X)$ are obtained from eqs.(102) and (103) as

$$\overline{Q}=\overline{U}\,\overline{H}=\overline{R}\,X \qquad (124)$$

$$\frac{d\overline{H}}{dX}=\frac{-2\overline{R}^2\overline{H}X}{\left(\overline{H}^3/F_0^2\right)-\overline{R}^2X^2} \qquad (125)$$

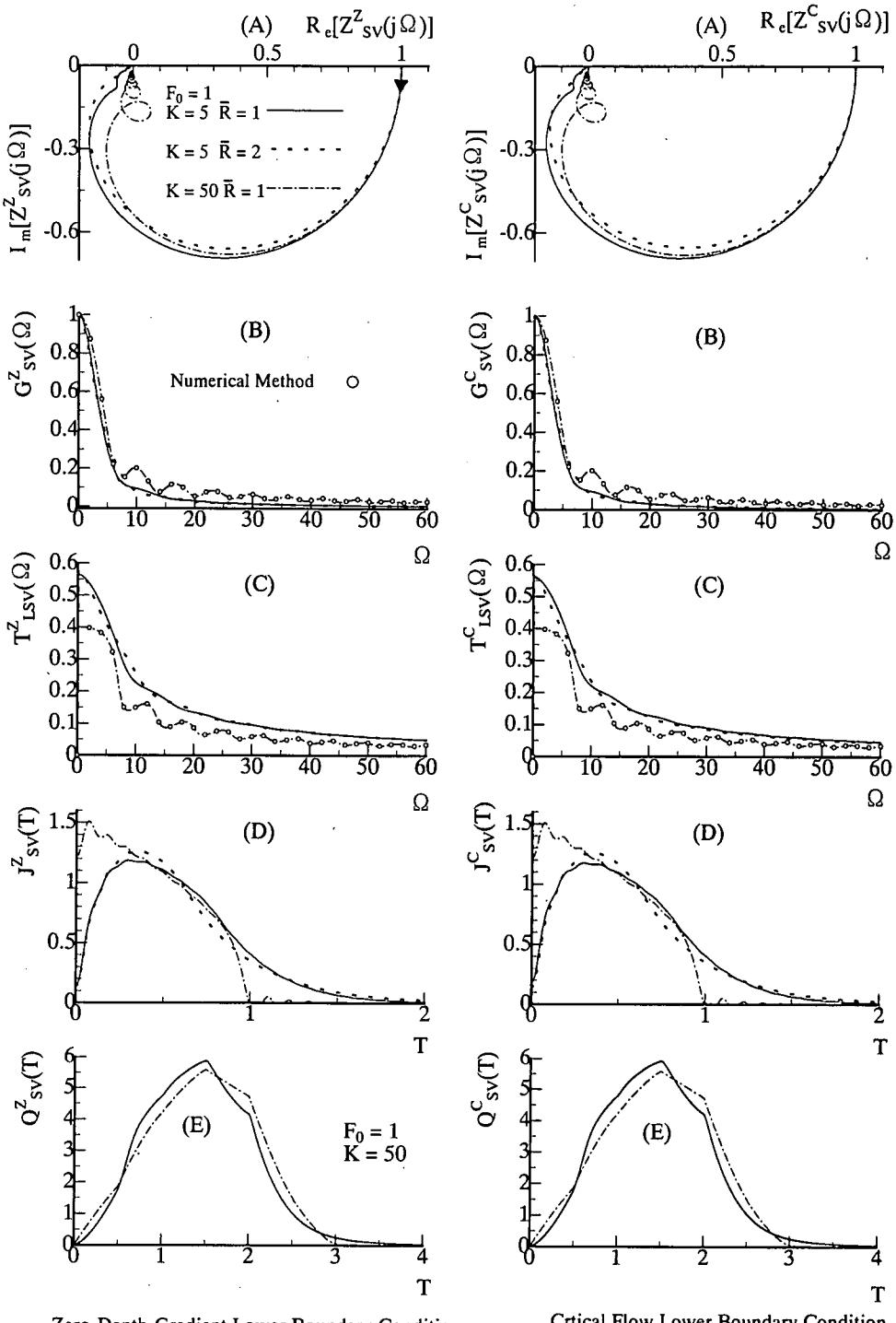

Zero-Depth-Gradient Lower Boundary Condition

Crtical Flow Lower Boundary Condition

Fig.6 St.Venant wave model

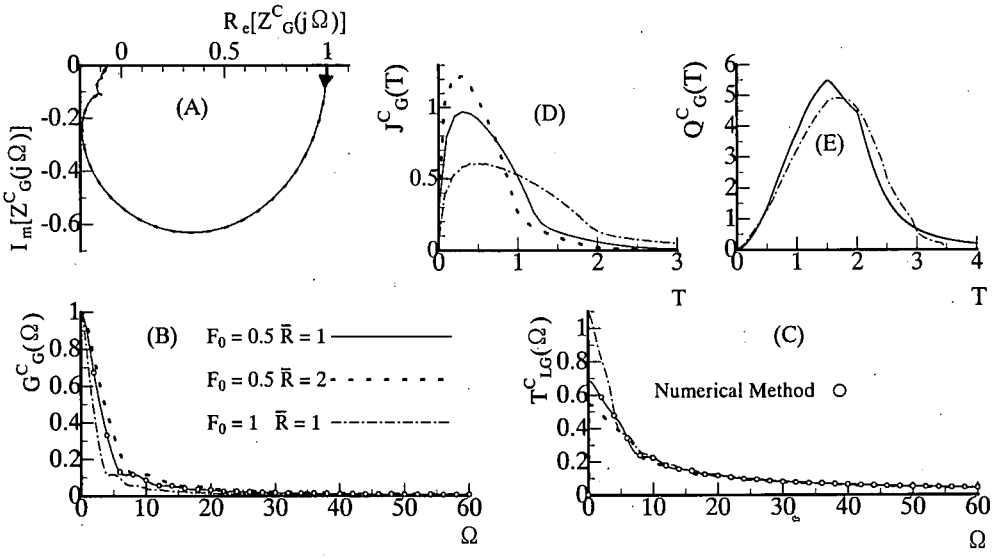

Fig.7 Critical flow lower boundary condition – Gravity wave model

Also, from eqs(104) and (105) we can obtain

$$\frac{dC}{dX} + j\Omega B = A \tag{126}$$

$$\frac{dB}{dX} = \left\{\overline{H}F_0^2\left(-2\overline{R}C - j\Omega C\overline{H}\right) + 2F_0^2\overline{Q}\left(j\Omega B\overline{H} - \overline{R}B - A\overline{H}\right) + \left(2F_0^2C\overline{Q} - 3B\overline{H}^2\right)d\overline{H}/dX\right\}/\left(\overline{H}^3 - F_0^2\overline{Q}^2\right) \tag{127}$$

Eq.(128) is obtained after eliminating B from eqs.(126) and (127).

$$\frac{d^2C}{dX^2} + f_1\frac{dC}{dX} + f_2C = f_3 \tag{128}$$

f_1, f_2, f_3 are as defined by eqs.(107~109) with $K = 0$. Eq.(74) suggests that

$$C(0) = 0 \tag{129}$$

a) Zero-depth-gradient condition

There is no solution for eqs.(121) and (122) which satisfies this lower boundary condition.

b) Critical flow condition

This condition is defined by eq.(91). Equations (113) and (114) are used here. Equation (130) is derived by eq.(115).

$$\left[\frac{\partial Q}{\partial X}\right]_{X=1} = \left[-3R\right]_{X=1} \tag{130}$$

Equation (131) is derived from eq.(116).

$$\left[\frac{dC}{dX}\right]_{X=1} = -3A \tag{131}$$

The equivalent frequency transfer function between $R(T)$ and $Q(T,1)$ is defined as

$$Z_G(j\Omega) = \frac{C(1)}{AL} \tag{132}$$

The gain and time lag functions are

$$G_G^C(\Omega) = \left|Z_{SV}(j\Omega)\right| \tag{133}$$

$$T_{LG}^C(\Omega) = \frac{Arg[Z_{SV}(j\Omega)]}{\Omega} \tag{134}$$

Figure 7 (A),(B),(C) and (D) show the vector locus, gain, time lag and impulse response functions for critical flow lower boundary conditions with $F_0 = 0.5$ and $\overline{R} = 1$ (solid line), $F_0 = 0.5$ and $\overline{R} = 2$ (dotted line), and $F_0 = 1$ and $\overline{R} = 1$ (dashed line). The circles in (B) and (C) indicate numerical results as explained before. The numerical results agree with theoretical ones. **Fig.7** (E) shows a comparison between solutions obtained from eqs.(121), (122) (solid line) and the solution obtained from impulse response function (dashed line) using the previously mentioned rainfall. The solutions show good agreement.

4. APPLICATION OF EQUIVALENT RESPONSE METHOD TO NONLINEAR SYSTEM

(1) Model criterion of St. Venant equation and its related models

In this paper, we compare the impulse response function between the St.Venant model and its related models for a range of Froude number ($0.1 \le F \le 2$) and kinematic wave number ($1 \le K \le 20$) with two types of lower boundary conditions. The adopted statistical criterion for

comparison is expressed by

$$S(F_0,K)=\sqrt{\frac{1}{N}\sum_{1}^{N}(J_S-J_X)^2} \qquad (135)$$

J_S : impulse response function of the St.Venant
J_X : impulse response function of other models
N : the total number of points taken at regular ΔT intervals along J_S and J_X for every $K-F_0$ pair.
S : normalizing statistical criterion
The value $S=0.2$ was selected as the limit, because at this value kinematic, diffusion, and gravity wave solutions cease to be good approximations for the St.Venant equations. Thus

$$\begin{cases} S \le 0 & \textit{Good approximation for St.Venant} \\ S > 0 & \textit{Not good} \end{cases} \qquad (136)$$

We calculated two types of relative errors between the St.Venant and its related models using a triangular rainfall, with maximum rainfall intensities ($R_p=0.5,1.0,2.0$) and duration ($T_p=3$), as shown in **Figure 8**, in order to check the validity of the limit $S=0.2$, as follows:

$$E_Q=\frac{Q_S(T_S,1)-Q_X(T_S,1)}{Q_S(T_S,1)} \qquad (137)$$

$$E_T=\frac{T_S-T_X}{T_S} \qquad (138)$$

E_Q : relative error for peak discharge
E_T : relative error for time to peak
Q_S,T_S : peak discharge and its time for St.Venant
Q_X,T_X : peak discharge and its time for other models
All cases that we calculate satisfy the conditions $E_Q \le 0.04$ and $E_T \le 0.05$. **Figure 9** shows the partition of the $K-F_0$ field into zones each of it indicates the validity of each model, where S.V., D, K, G, and U indicate the St.Venant, Diffusion (□), Kinematic (●), Gravity (▪) and Undetermined zone (○), for $\bar{R}=0.5,1,2$, with zero depth gradient lower boundary condition (A), (B) and (C), and critical flow condition (D), (E) and (F), whereas the dashed line shows the results from a previous work obtained for $\bar{R}=1$.

Our results show that the criteria proposed by Woolhiser and Liggett (1967) and by Morris and Woolhise (1980) are necessary but not sufficient. Also, they differ from that obtained by Daluz (1982) in the following aspects:

1) For $K<9$, full St.Venant must be used, and lower boundary condition is not important, except for $K \le 5$ and $F_0<1$ where gravity model might be used.
2) For $K \ge 10$, the diffusion and kinematic zones are similar, and the choice between St.Venant and diffusion model depends on F_0 values.
3) Also Daluz's results did not realize that St.Venant is only applied for $\bar{H}_Z(1) \ge (F_0R)^{2/3}$

We can conclude that for high rainfall intensities, kinematic wave model might be applicable only for large values of F_0, and K, and St.Venant is a dominant model in F_0-K field and vice versa.

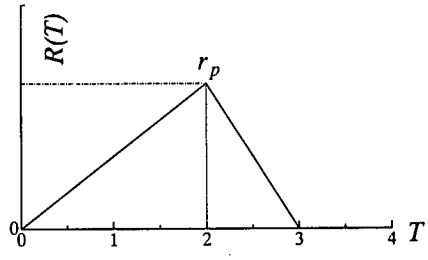

Fig.8 Adopted triangular rainfall for checking S value

(2) Application to real runoff analysis

In this section, we point out the possibility of an application of EFRM to real runoff analysis.
If we assume that a runoff system is described by a nonlinear lumped parameter model such as eqs.(20) and (21) and hydrological data such as rainfall and discharge are available, then we can calculate $Z(j\Omega)$ between $r(t)$ and $q(t)$.

$$Z(j\Omega)=\frac{Q(j\Omega)}{R(j\Omega)} \qquad (139)$$

$$Q(j\Omega)=\int_0^\infty q(t)e^{j\omega t}dt \qquad (140)$$

$$R(j\Omega)=\int_0^\infty r(t)e^{j\omega t}dt \qquad (141)$$

$r(t)$ and $q(t)$: effective rainfall and direct discharge
Assume a second order differential equation to describe a runoff system defined by

$$f_1(\bar{r})\frac{d^2q}{dt^2}+f_2(\bar{r})\frac{dq}{dt}+q=r \qquad (142)$$

The coefficient of eq.(142) should be the function of $\bar{r}$ according to the previous section.
Real and imaginary parts of $Z(j\Omega)$ are defined by eqs.(143) and (144).

$$R_e(Z)=\frac{R_e(Q)R_e(R)-I_m(Q)I_m(R)}{R^2_e(R)+I^2_m(R)} \qquad (143)$$

$$I_m(Z)=\frac{R_e(Q)I_m(R)+I_m(Q)R_e(R)}{R^2_e(R)+I^2_m(R)} \qquad (144)$$

Eqs.(143) and (144) lead gain and time lag as defined before, which in turn yield $f_1(\bar{r})$ and $f_2(\bar{r})$ as

$$f_1(\bar{r})=\frac{1}{\omega^2}\left\{1-\frac{1}{G(\omega)\sqrt{1+\tan^2\{\omega T_L(\omega)\}}}\right\} \qquad (145)$$

$$f_2(\bar{r})=\left\{\frac{\tan\{\omega T_L(\omega)\}}{\omega G(\omega)\sqrt{1+\tan^2\{\omega T_L(\omega)\}}}\right\} \qquad (146)$$

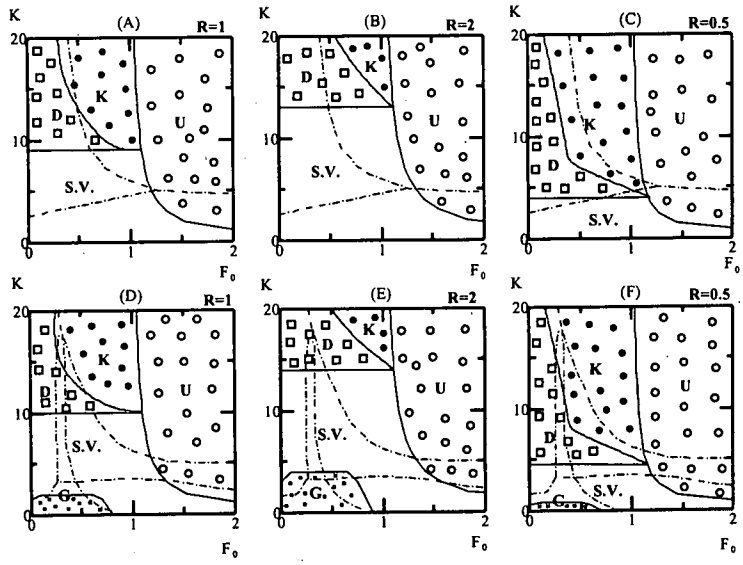

Fig.9 Partition of K - F_0 field into validity zones.
S.V., D, K, G, U indicate St.Venant, Diffusion (□), Kinematic (●), Gravity (■),and undetermined zone (○)
(A), (B), (C) for Zero-depth- gradient lower boundary condition
(E), (F), (G) for Critical flow lower boundary condition

Figure 10 (A), (B) and (C) show the vector locus, gain, and time lag functions obtained from the observed rainfall (D) and discharge (E) (solid line) at Maruseppu (drainage area 802 Km^2 Sep. 16^{th} 1998), Yubetsu River , Hokkaido. Also, **Fig.10** (F) and (G) show f_1 and f_2. If eq.(142) completely describes the runoff system, their coefficients are independent of frquency ω. **Fig.10** (F) and (G), however, suggest that eq.(142) describes only the low frequency components of the runoff system. **Fig.10** (E) shows a comparison of the observed discharge (solid line) and the computed one (dashed line) by eq.(142) and rainfall as shown in **Fig.10** (D) using average $\bar{f}_1$ and $\bar{f}_2$ for a range of $0 \le \omega \le 0.2$, where

$$\bar{f}_1 = 25.92 \ (hr^2) \quad ; \quad \bar{f}_2 = 8.85 \ (hr)$$

Fig.10 (E) shows that it is possible to neglect frequency components higher than $\omega = 0.2$.

As we analyze only one flood event using the observed data, many cases should be analyzed to obtain general results. A real catchment basin consists of two elements, slopes and channels. The equivalent frequency transfer function in the previous section describes the relation between the input and output for one element. Let us consider a simple basin that consist of two slopes and one channel as shown in **Figure 11**. We adopt the kinematic wave model for convenience.

Slope-1

$$\frac{\partial h_{s1}}{\partial t} + \frac{\partial q_{s1}}{\partial x} = r \qquad 0 \le x \le l_1$$

$$q_{s1} = \alpha_1 h_{s1}^{p_1} \tag{147}$$

Slope-2

$$\frac{\partial h_{s2}}{\partial t} + \frac{\partial q_{s2}}{\partial x} = r \qquad 0 \le x \le l_2$$

$$q_{s2} = \alpha_2 h_{s2}^{p_2} \tag{148}$$

Channel

$$\frac{\partial a}{\partial t} + \frac{\partial q_c}{\partial y} = q_{s1}(t,l_1) + q_{s2}(t,l_2) \qquad 0 \le y \le l_c$$

$$q_c = \beta a^{p_3} \tag{149}$$

α, β and p : constants
l_1, l_2 and l_c : length of slope-1, slope-2, and channel
h_s and q_s : water depth and discharge
a and q_c : cross sectional area and discharge
It is possible to define the frequency transfer function of eqs. (147), (148) and (149).
Eqs.(147), (148) and (149) are transferred to

$$Q_{s1}(j\omega,l_1) = l_1 Z_1(j\omega) R(j\omega) \tag{150}$$

$$Q_{s2}(j\omega,l_2) = l_2 Z_2(j\omega) R(j\omega) \tag{151}$$

$$Q_c(j\omega,l_c) = l_c(l_1 + l_2) Z_3(j\omega) R(j\omega) \tag{152}$$

$Z_1(j\omega), Z_2(j\omega)$ and $Z_3(j\omega)$: frequency transfer function of eqs.(150), (151) and (152) respectively
$Q_{s1}(j\omega), Q_{s2}(j\omega)$ and $Q_c(j\omega)$: Fourier transformed functions of $q_{s1}(t,l_1), q_{s2}(t,l_2)$, and $q_c(t,l_c)$
The whole frequency transfer function is defined as

$$Z(j\omega) = \frac{1}{l_1 + l_2} Z_3(j\omega)\{l_1 Z_1(j\omega) + l_2 Z_2(j\omega)\} \tag{153}$$

It is possible to calculate the total frequency transfer function based on sub-basin ones.

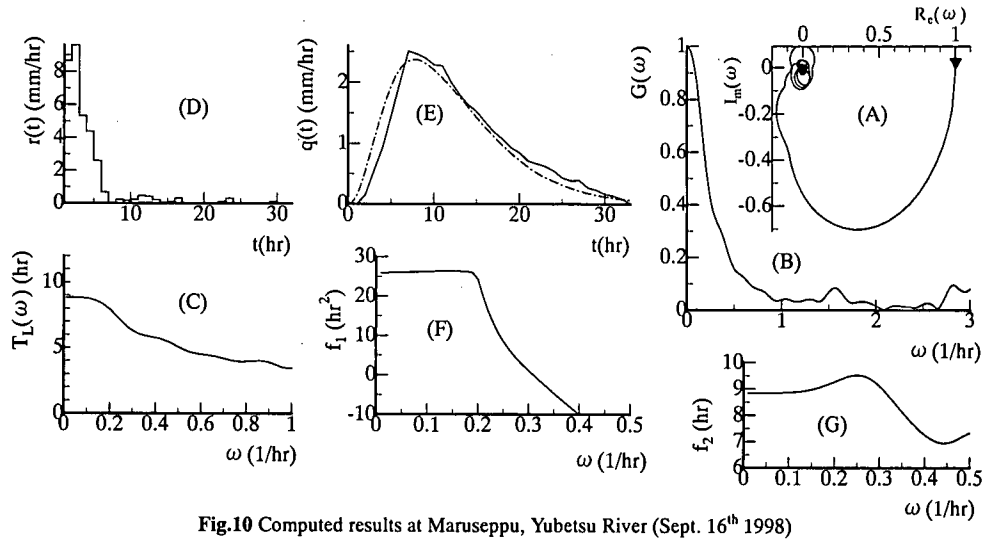

Fig.10 Computed results at Maruseppu, Yubetsu River (Sept. 16th 1998)

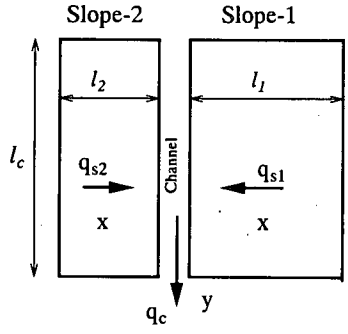

Fig.11 A simple runoff system

5. CONCLUSION

The distributed parameter runoff models, St.Venant, gravity, diffusion, and kinematic models, and the lumped parameter runoff model, the storage function model, were analyzed using the EFRM.

It was verified that all of the adopted non-linear runoff models can be converted into semi-linear runoff ones. The word "semi-linear" means that the obtained equivalent impulse response functions depend on the average rainfall.As the average rainfall increases, the gain increases and time lag function decreases. This phenomenon indicates that runoff from each model approaches its rainfall input and the equivalent response function approaches the unit impulse function as the average rainfall increases.

We have presented a more practical validity diagram for the St.Venant equations and related models on the $K-F_0$ plane using the equivalent impulse response function.

Finally, we have suggested the possibility of a new application of the EFRM to real runoff analysis.

REFERENCES

1) Woolhiser, D.A. and Liggett, J.A.: Unsteady, one-dimensional flow over a plane- The rising hydrograph, Water Resour. Res., Vol.3, pp.753-771,1967.
2) Morris, E.M. and Woolhiser, D.A.: Unsteay one-dimensional flow over a plane: partial equilibrium and recission hydrographs, Water Resour. Res.,Vol.16, pp.355-360,1980.
3) Daluz Vieira, J.H.: Conditions governing the use of approximations for the Saint-Venant equations for shallow surface water flow, Journal of Hydrology, Vol.60, pp.43-85,1983.
4) Fujita, M., Kudo, M., Nako, T. and Hashimoto, N.: Stochastic response of storage function model, JSCE, No.515/II-31, pp.1-11,1995.
5) Tanaka, G., Fujita, M. and Hamouda, L.: Application of extended frequency response method to a runoff system, Annual Journal of Hydraulic Engineering, JSCE, Vol.42, pp.181-186,1998.
6) Tanaka, G., Fujita, M., Kudo, M. and Uchijima, K.: Comparison between kinematic wave model and storage function runoff model-Frequency characteristic and stochastic characteristics-,J. of Hy. Co., JSCE, No.614/II-46, pp.21-36, 1999.
7) Fujita, M.: Study on storage function model considering the effect of slope length, J. of Hy. Co., JSCE, No.314, pp.75-86, 1981.
8) Hoshi, K. and Yamaoka, I.: Relationship between storage function and kinematic wave model, Annual Journal of Hydraulic Engineering, JSCE, pp.273-278,1982.

(Received May 29,2000)

等価周波数応答法による非線形流出系の解析

Luai HAMOUDA・藤田睦博

本研究は，Saint Venant 式とこれから派生する diffusion wave, gravity wave と kinematic wave 式を対象に，降雨量と斜面末端あるいは河道末端からの流出量間の等価周波数伝達関数や等価インパルス応答関数を求める手法を提案した．一方，これまで Saint Venant 式より得られるフルード数 F_0 とキネマテックウィブ数 K の２つの無次元パラメタを用いて，F_0～K 平面上でモデルの敵合度が検討されてきた．これらは，一定の降雨量を採用し各モデルより計算される上昇期のハイドログラフを比較している．本研究では，各モデルの等価インパルス応答関数を比較し，降雨波形に依存しない F_0～K 平面上でモデルの敵合度の判定法を示した．更に，等価周波数伝達関数や等価インパルス応答関数を実流域の流出解析に応用する手法についても検討している．